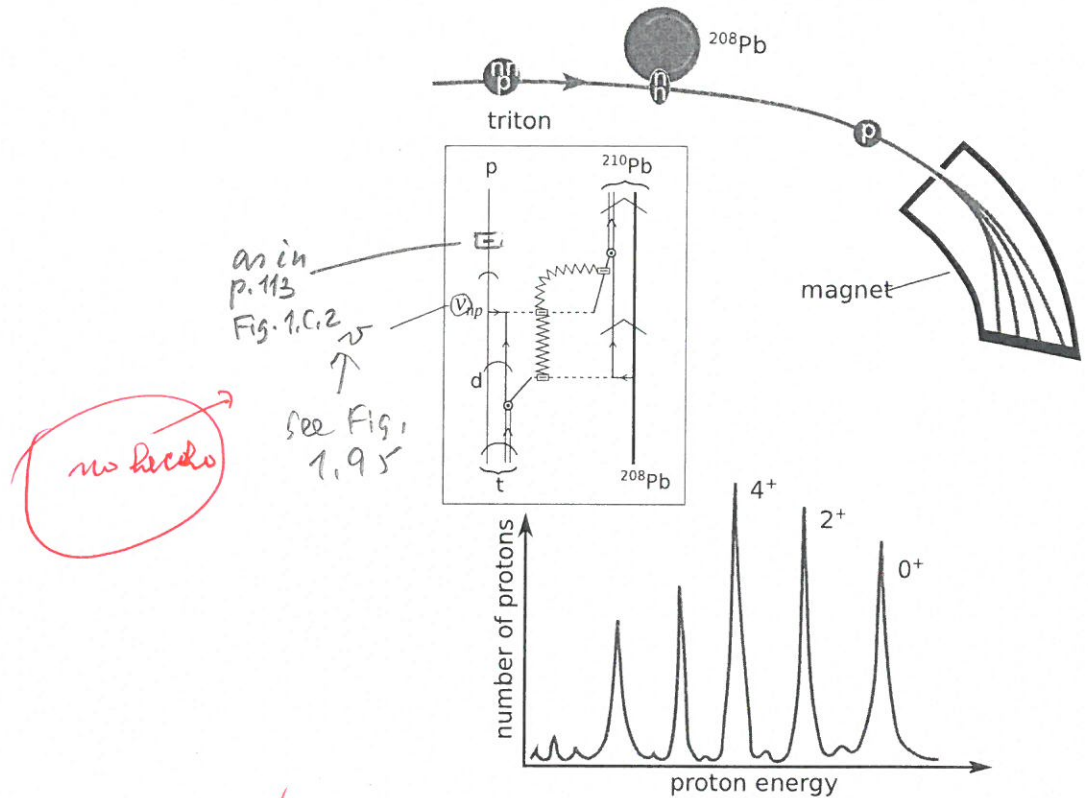


✓ Figure 1.1.2: (Color online) Schematic representation of the one-nucleon transfer reaction  $^{208}\text{Pb}(d, p)^{209}\text{Pb}$  populating the valence single-particle states of  $^{209}\text{Pb}$ . In the inset a schematic NFT( $r+s$ ) diagram describing the process is shown. Curved arrows describe the projectile and outgoing particle moving in the continuum. The short horizontal arrowed line labeled  $v_{hp}$  represents the proton-neutron interaction inducing the transfer process (dashed horizontal line) while the dashed open rectangle indicates the Particle Recoil Coupling (PRC) vertex. That is, the coupling of the relative motion to the recoil process described in terms of a jagged line. This information is carried out in the center of mass system by the outgoing particles in the final channel. Within this context the jagged line is involved in a virtual process (insets (I) and (II)). The energy and momentum of the outgoing proton reflects the recoil, the  $Q$ -value of the reaction and the excitation energy of the final state as analyzed in the magnet and recorded in the particle detector (a,b,c) (after Mottelson (1976b)).

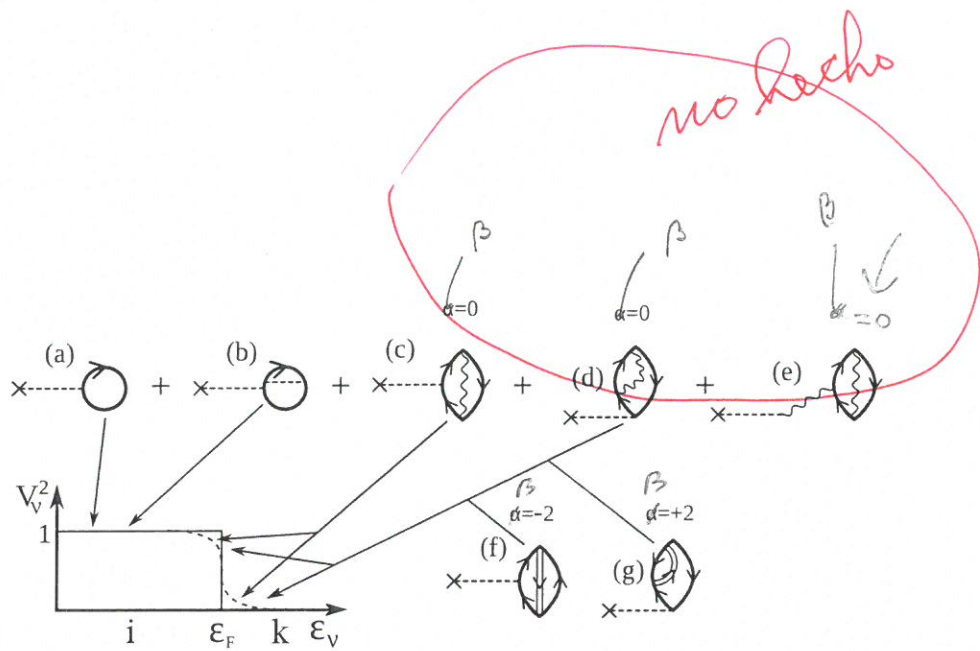


✓ Figure 1.1.3: (Color online) Schematic representation of the two-nucleon triton reaction  $^{208}\text{Pb}(t, p)^{210}\text{Pb}$  process populating the ground state  $0^+$ , and two  $p$ -excited states  $2^+$  and  $4^+$ . That is, monopole, quadrupole and hexadecapole addition modes (multipole pairing vibrations) of  $^{208}\text{Pb}$  (App. 6.F; see also D. and Broglia (2005) Sect. 5.3.1 p. 108). In the inset a NFT( $r+s$ ) diagram (successive) transfer process is displayed. The jagged line brings information about the outgoing nuclei in the exit channel (CM system), of the change in scale of the asymptotic outgoing waves with respect to the incoming ones, concerning different mass partitions (recoil) of summed value  $2m$ . In the standard setup (in terms of a cartoon, this information is carried out to the detector by the outgoing proton (see App. 1.C, Sect. 1.C.3) (after Mottelson (1976b)).

(app. 1D up)

Concerning the apparent  
non-linearity (direct coupling  
of two recoil modes, see Sect. 1.C.3;  
see also Fig. 1.7/10, last line).

captions



✓ Figure 1.2.2: Schematic representation of the Fermi distribution. The sharp, continuous line drawn step function schematically represents the Hartree–Fock occupation numbers. The associated nuclear density measured with the help of an external field (cross attached to a dashed line) through processes of type (a) (Hartree: H) and (b) (Fock: F) is expected to display a diffusivity of the order of the strong force range. Zero Point Fluctuations (ZPF) associated with collective particle–hole state, i.e. processes with transfer quantum number  $\beta = 0$  (Bohr (1964)) and shown in (c), (d) and (e), and with pairing vibrations, i.e. pair addition (graph (f)) and pair removal modes (graph (g)), smooth out the occupation numbers around the Fermi energy (dashed curve) and lead to a nuclear density of larger (dynamical) diffusivity than that associated with HF. One- and two-particle strengths which in this (mean field) approximation are found in a single  $A$ -mass system, are a result of ZPF ( $\beta = 0, \pm 1, \pm 2$ ) distributed over a number of nuclei ( $A, A \pm 1, A \pm 2$ ) (see also App. 4.H, Fig. 4.H.1).

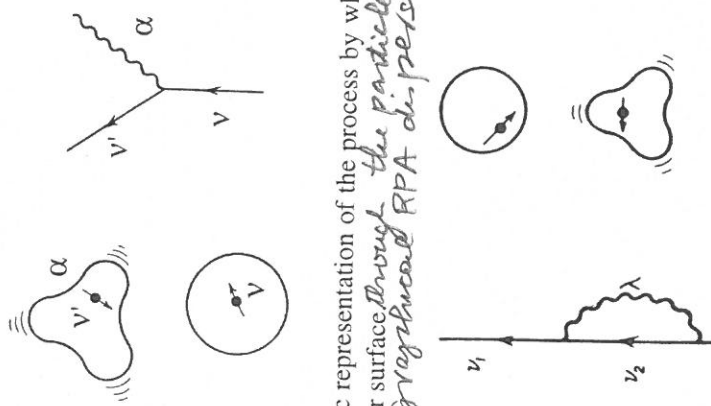
(vibrations)

as

### 1.3. PARTICLE-VIBRATION COUPLING

31

$$\chi - \underbrace{\alpha}_{\equiv} = \underbrace{\alpha'}_{\chi'} + \underbrace{\alpha''}_{\chi''}$$



✓ Figure 1.3.1: Schematic representation of the process by which a nucleon excites vibrations of the nuclear surface through the particle-vibration coupling vertex. In the inset, the ground-state RPA displacement relation of the nucleons determines the motion of the collective mode  $\alpha$ , which is enlarged (see Figure ...)

low-lying  
e.g. the Octupole vibration of  $^{208}\text{Pb}$

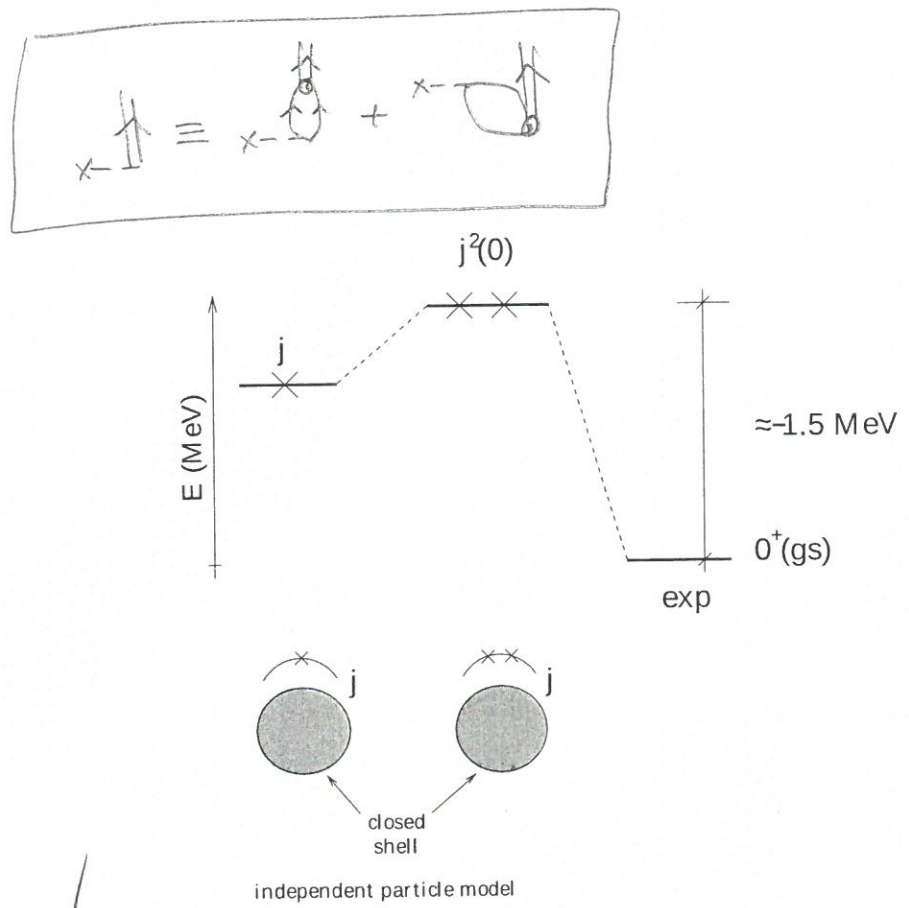


Figure 1.3.10: Schematic representation of the predictions of the independent particle model for one- and two-particles outside closed shell, in comparison with the experimental findings (e.g. for the case of  $^{210}\text{Pb}$ , where  $j = g_{9/2}$ ).

In the next, the graphical RPA dispersion relation leading ~~to~~ to  $^{140}\text{Pb}(\text{gs})$  is shown (See Preface...)

## 1.7. NUCLEAR FIELD THEORY FOR PEDESTRIANS

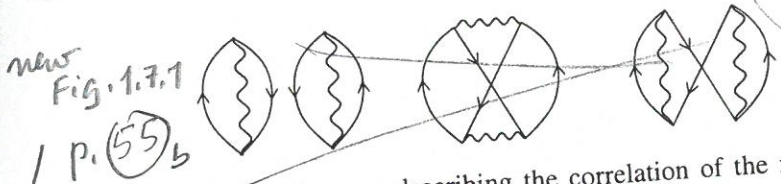


Figure 1.7.1: Oyster diagrams describing the correlation of the nuclear ground state associated with the ZPF of collective particle-hole-like excitations, and Pauli principle correction processes in which fermions are exchanged. This is in keeping with the fact that the collective modes are built out of the particle degrees of freedom (see e.g. Fig. 1.D.1).

In (a) we show two of such diagrams.  
In (b) and (c) we display a symmetrized (boson exchange), and antisymmetrized (fermion exchange) correction to (a), while (d) contains a simultaneous boson and fermion exchange.

A - A  
p. 55 a

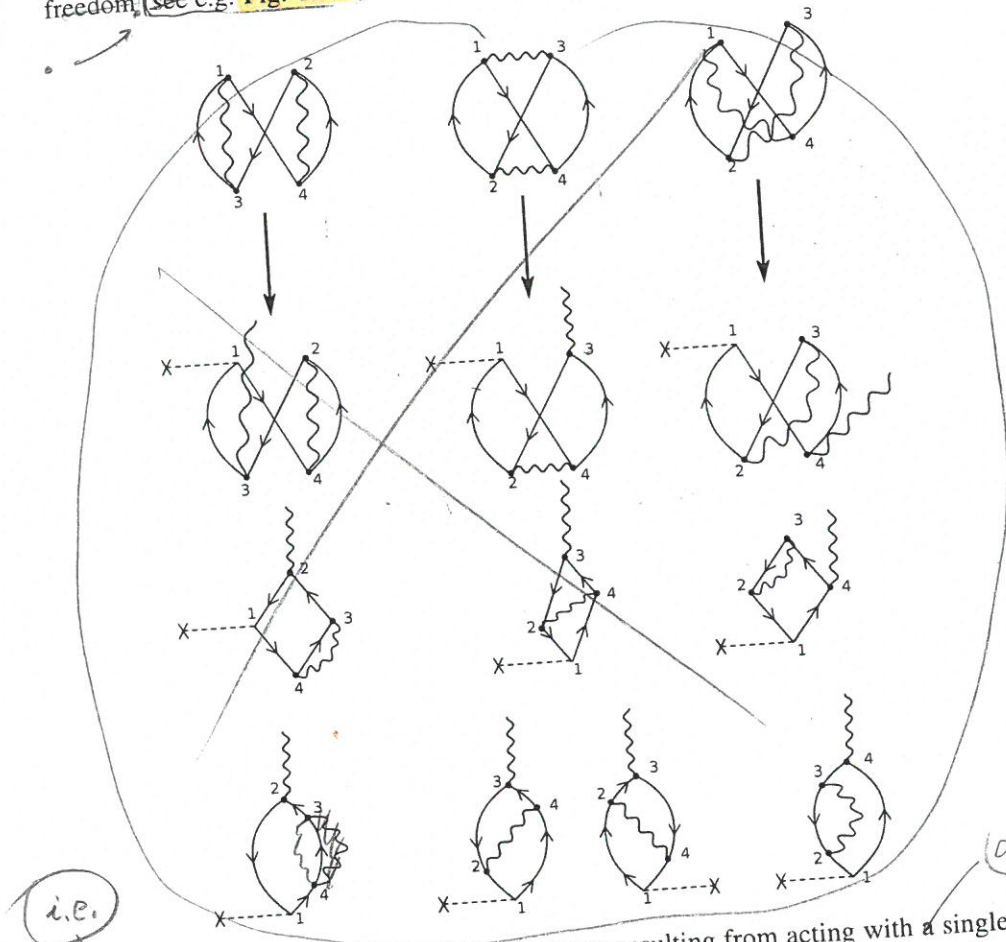


Figure 1.7.2: Some of the possible outcomes resulting from acting with a single-particle field, e.g. that associated with inelastic processes (represented by a horizontal dashed line starting with a  $\times$ ), on the Pauli-corrected ZPE oyster diagrams associated with collective ( $p-h$ ) excitations of the nuclear vacuum (see Fig. 1.7.1). Within this context one returns to the question of renormalization mentioned in the text (see end of Sect. 1.1 and Sect. 1.4, see also Idini et al. (2015), Broglia et al. (2016), Barranco et al. (2017a); see also Sect. 6.5).

(B) - (B)  
CROSS  
from P. 55 a  
with the ZPF of a nucleus associated with particle-hole correlated vibrations.

ground state

The last diagram describes

(55)

a

(B) The diagrams of the first row result by intervening the virtual process shown in Fig. 1.7.1 (c) and eventual time ordering. Similar for those of the second row but in connection with diagram (d) of Fig. 1.7.1. The boxed processes correspond to particle self-energy (first row) and vertex correction (second row). Reversing the sense in which the fermions (arrowed lines) circle the loop from anti-clockwise to clockwise, one obtains two new graphs. The complete set of processes obtained in this way are shown in the third and last row, constitute a sum rule conserving set of diagrams <sup>(see text)</sup> as discussed in connection with Fig.

Caption Fig. 1.7.2

(B)

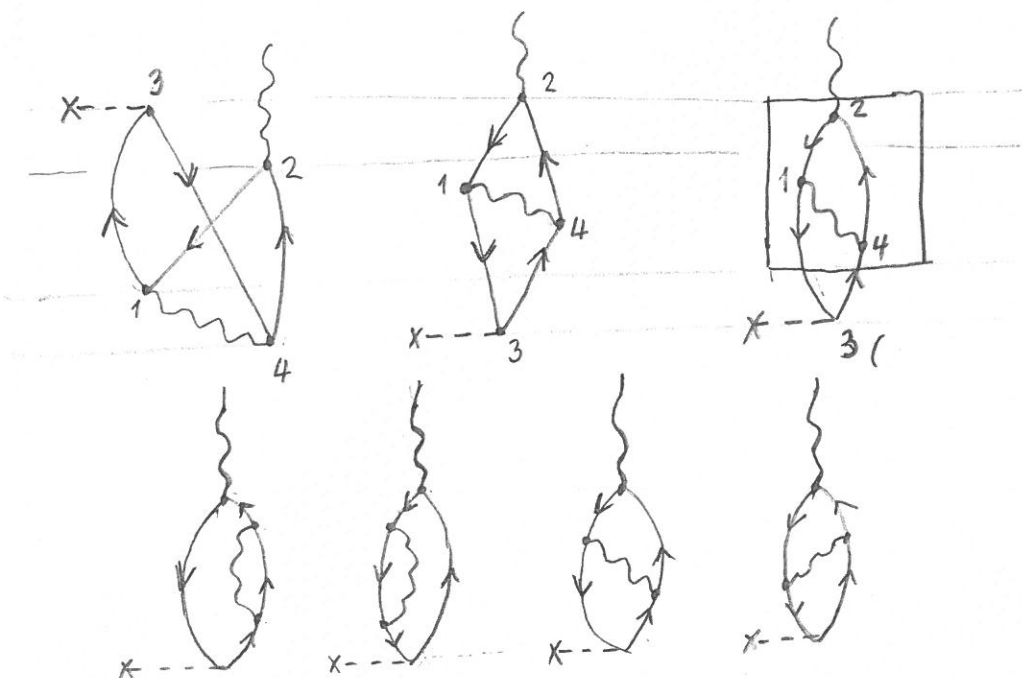
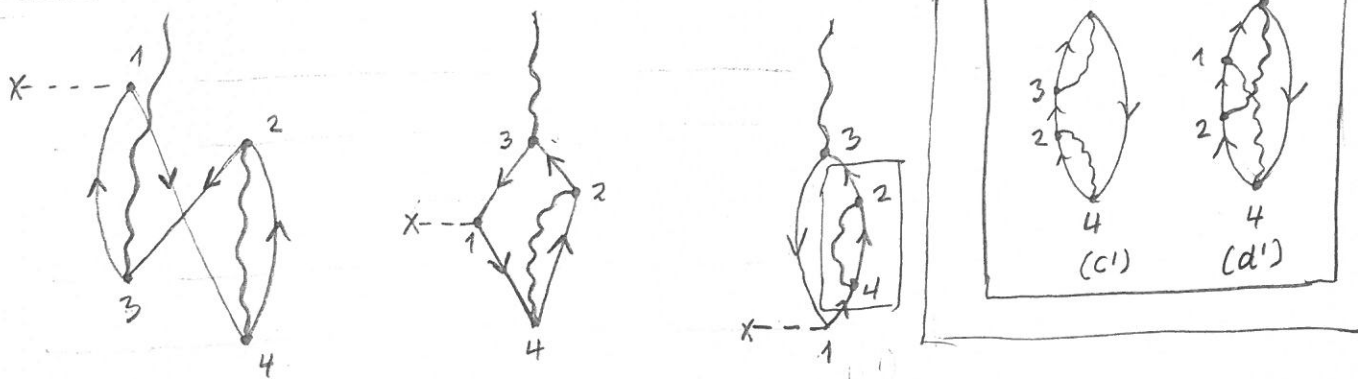
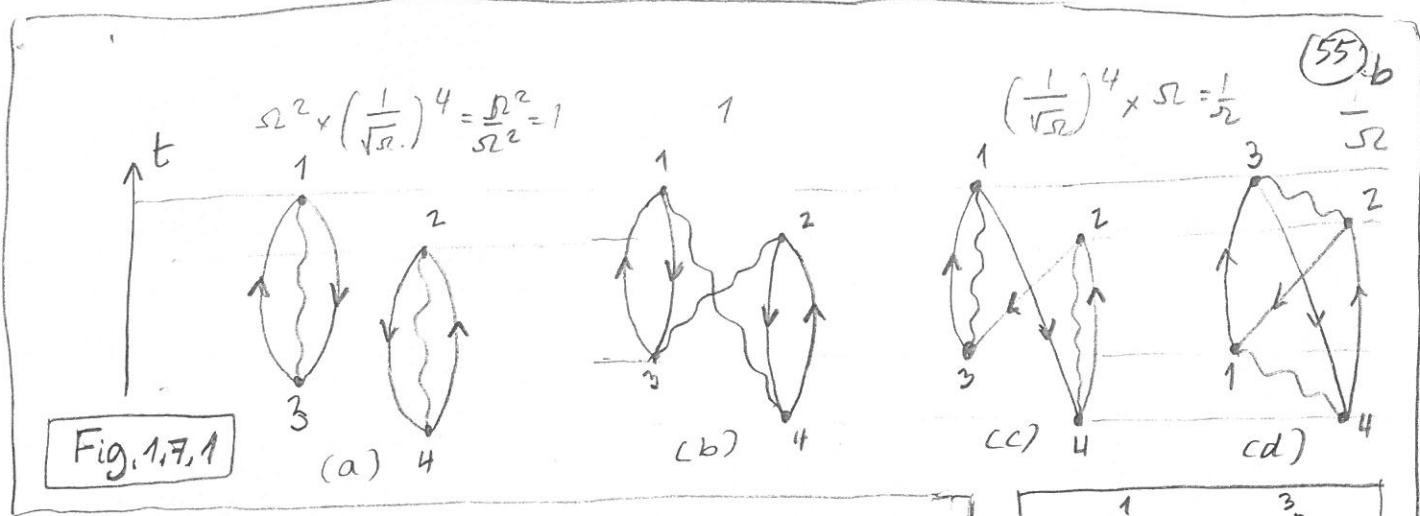
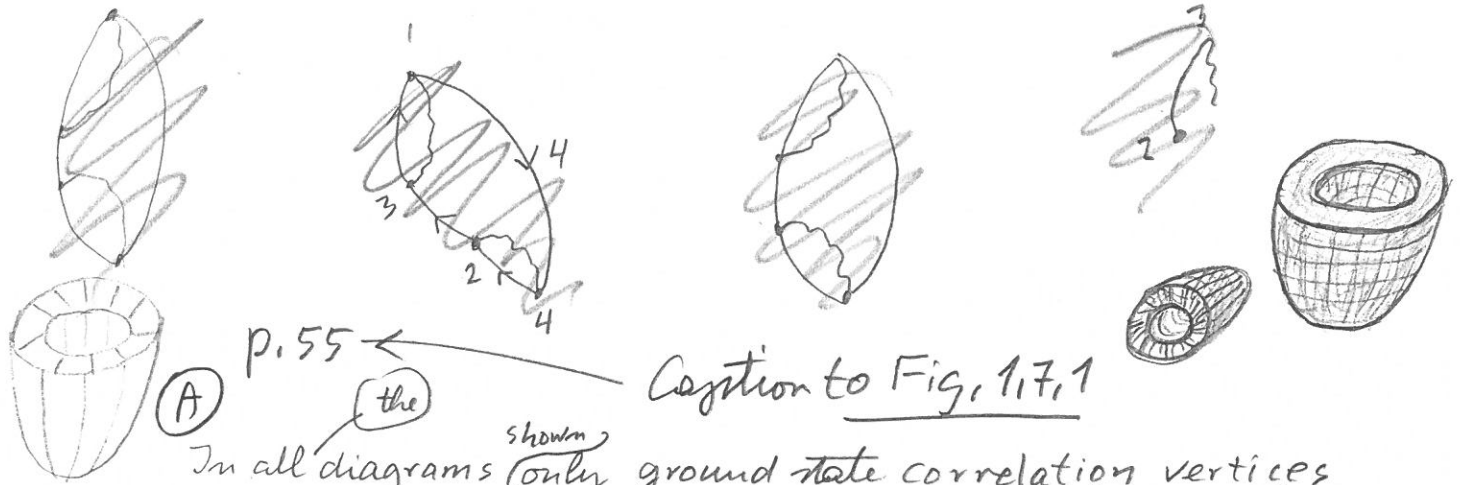


**Fig. 1.7.2**



Caption to Fig. 1.7.1

In all diagrams (only) ground state correlation vertices are present, they are connected with the  $\chi_{ki}^{\alpha}$ -components ( $\epsilon_k > \epsilon_F$ ,  $\epsilon_i \leq \epsilon_F$ ) of the RPA wavefunction describing the collective mode (wavy line). While this is so for ~~any~~ any time ordering ~~in~~, i.e. the sequence ~~in~~ with which the particle-vibration coupling vertices (black dot) appear (time is assumed to ~~run~~ run as indicated to the left of (a)), in the case of the processes shown in (a) and

(b), this is not the case in connection with processes (c) and (d) as can be seen from the corresponding diagrams (c') and (d') shown in the inset. Because of Pauli principle (fermion exchange) between particles (holes) present (e.g. those of the first oyster diagram<sup>in (a)</sup>) and those involved in the collective mode (those of the second oyster diagram in (B)), the harmonic approximation is not valid any more. This is reflected in the ~~comparison~~ of scattering vertices

Caption to Fig 1.7.1

(A)



diagrammatically reflected

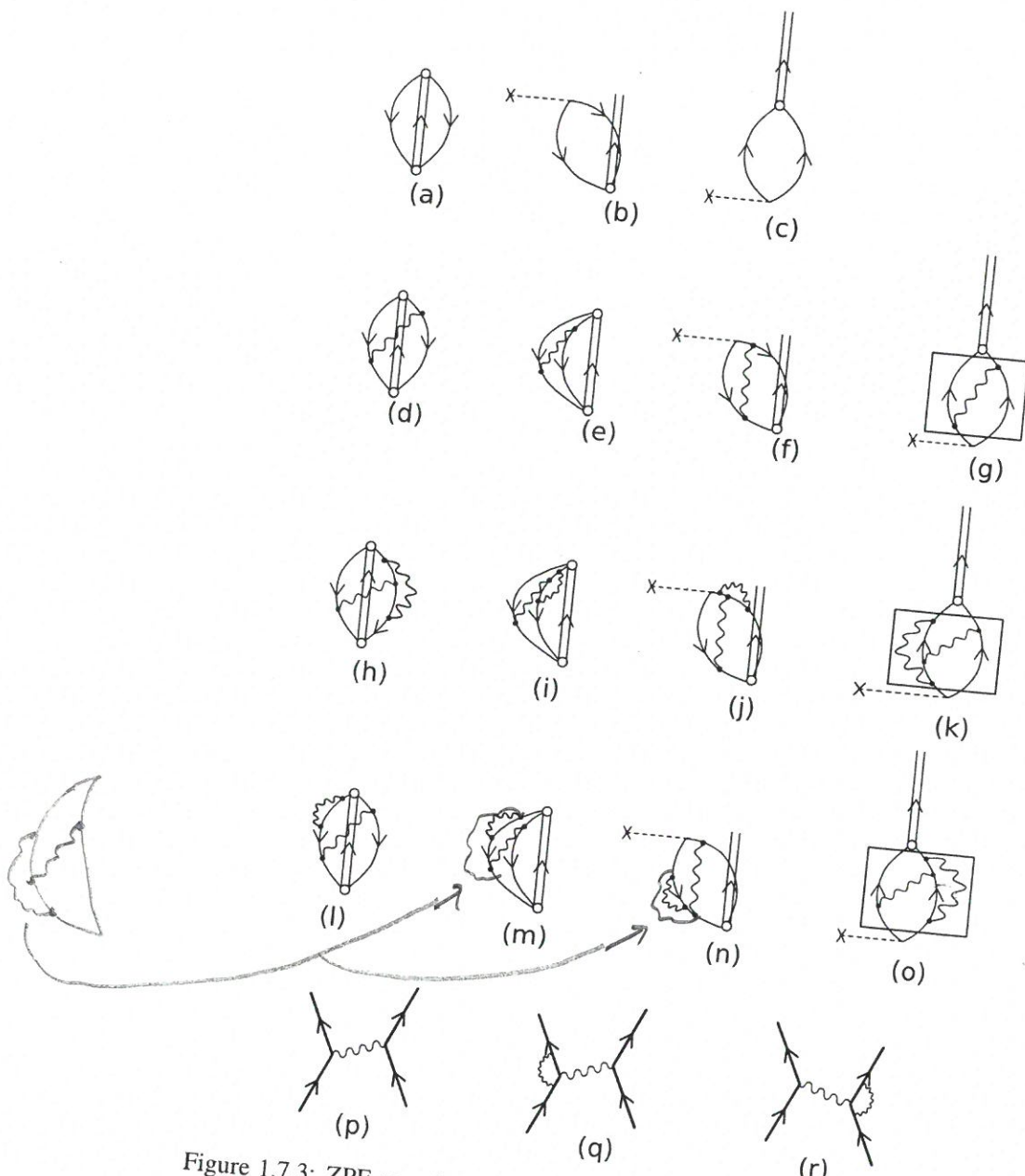


Figure 1.7.3: ZPF associated with the pair addition mode taking into account the interweaving of nucleons with density modes. The processes boxed in (g), (k) and (o), are associated with the induced pairing interaction (medium polarization effects); (p), (q), (r) resulting from the exchange of density modes between nucleons moving in time reversal states, including also vertex corrections. The two-nucleon stripping and pickup external field is labeled by a dashed horizontal line which starts with a  $\times$ . The possibility of using pairing vibrational modes as intermediate bosons contributing to the induced pairing interaction, not only in  $^1S_0$  channels but also in other channels (multipole modes) is discussed in App. 6.F. In particular, in connection with the possible presence of “vortex-like” pair addition modes, in exotic, halo nuclei, with  $J^\pi = 1^-$  and  $\beta = +2$  quantum numbers.

*mes grande*

### 1.C. TECHNICAL DETAILS NFT

111

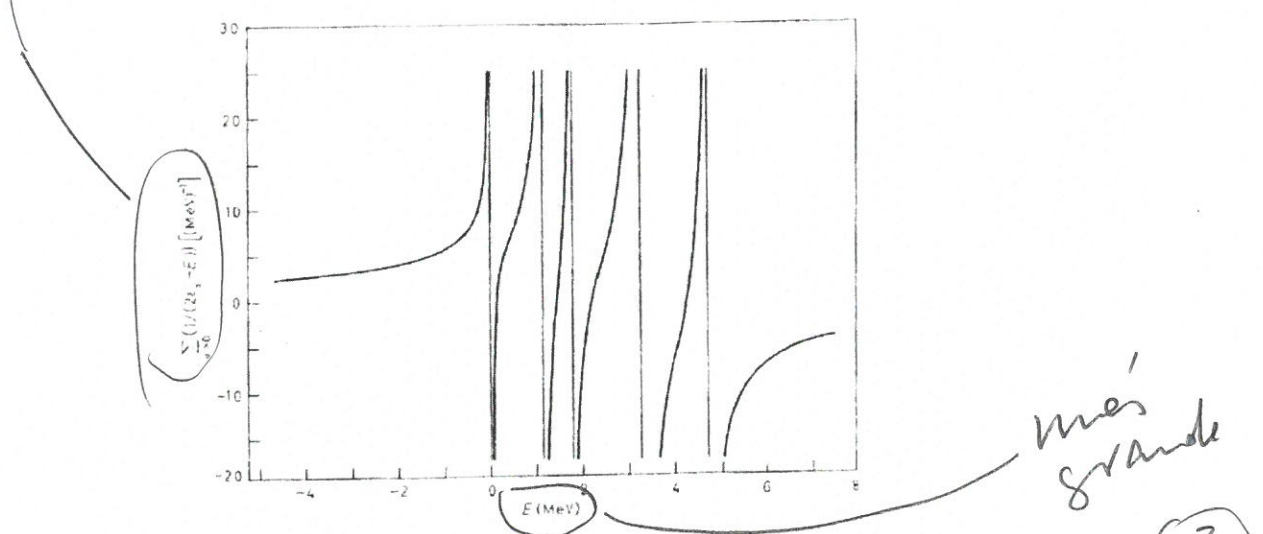


Figure 1.C.1: Dispersion relation for  $^{206}\text{Pb}$ . The single-hole states available to the two neutrons are  $p_{1/2}(0)$ ,  $f_{5/2}(0.57)$ ,  $p_{3/2}(0.89)$ ,  $i_{13/2}(1.63)$ ,  $f_{7/2}(2.34)$ . The label  $\alpha$  denotes the quantum numbers  $(j, m_j)$ .

*mes grande*

particle?

Le

Anticolo Ben Bayman  
Ref [12]

1 fm, and the  
of the nucleus  
was a large  
--- p. 57  
Varema

Varema  
β.B NP 15, 33 (1960)

and

$$\frac{1.81}{1.96} = 0.92$$

$$|II\rangle = -B|\alpha\rangle + A|\beta\rangle, \quad (1.C.6)$$

OK

with  $A^2 + B^2 = 1$ . This model would predict the value  $R = (\alpha/\beta)^2$  for the  $(t, \alpha)$  ratio.  $R(t, \alpha) = \sigma_I^{tr}/\sigma_{II}^{tr}$  and  $1/R$  for the  $(\alpha, \alpha')$  ratio  $R(\alpha, \alpha') = \sigma_I^{oct}/\sigma_{II}^{oct}$  (see Sect. 1.7.4). The ratio  $R_{th}(t, \alpha) = \frac{1.83}{2.25} = 0.81$  (against  $R_{exp}(t, \alpha) = 0.82$ ) and  $R_{th}(\alpha, \alpha') = \frac{2.5}{3.8} = 0.66$  (against  $R_{exp}(\alpha, \alpha') = 0.68$ ) is a direct consequence of the overcompleteness of the basis which is taken care of by the nuclear field theory. While this is a

3.7/1.5  
OK

Fig  
OK

Table  
~~3.8/2.7~~  
1.4

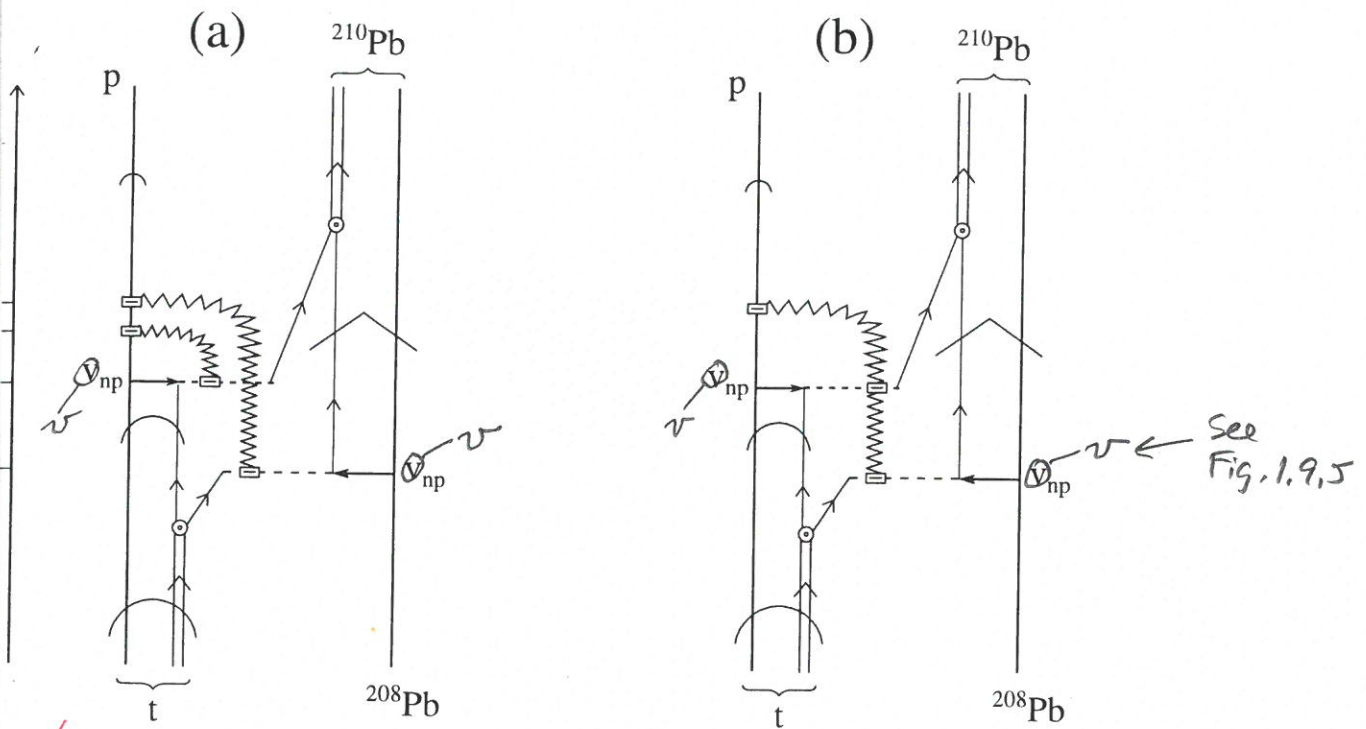
$$\frac{1.81}{1.96}$$

$$4.2/1.1$$

Table  
+ Fig

1.8/2.2 OK  
Table + Fig

OK as it is



✓ Figure 1.C.2: NFT( $r+s$ ) diagram describing the reaction  $^{208}\text{Pb}(t, p)^{210}\text{Pb}(\text{gs})$ . That is the population of the lowest energy, monopole pair addition mode of  $^{208}\text{Pb}$ . Concerning the different symbols used, we refer to Figs. 1.1.3 and 1.9.2. In particular concerning the recoil mode (jagged line) and the associated particle-recoil mode coupling vertex (dashed open rectangle) shown in ~~(a)~~. Also, of all the possible contributions associated with the different sequence of the processes taking place in this graph at times  $t_1, t_2, t_3$  and  $t_4$ , with the final outcome that the outgoing particle carries information to the detector of a transfer of two neutron masses. With this proviso in mind, and only for simplicity is that one replaces diagram (a) by diagram (b).

*May*

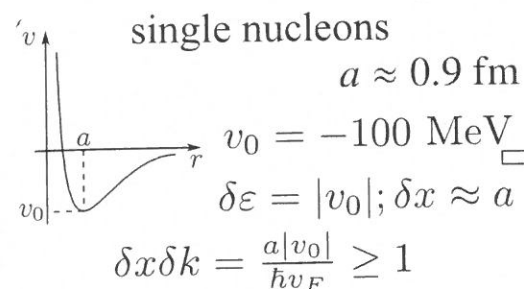
## Classical localization and quantal ZPF

$v_F/c$

$$\delta x \delta k \geq 1 \quad \varepsilon = \frac{\hbar^2 k^2}{2M} \quad \delta k = \frac{\delta \varepsilon}{\hbar v_F} \quad (v_F/c \approx 0.27)$$

structure

Independent motion of



quantity parameter

$$q = \left( \frac{\hbar v_F}{a |v_0|} \right) \approx 0.5 \lesssim 1$$

delocalization

$$\frac{\hbar^2}{m a^2 |v_0|}$$

emergent property: generalized rigidity in  
3D-space

how does a short range force lead to  
single-nucleon mean free paths  
larger than nuclear dimension?

$$2R \approx 20/k_F$$

quantal

fluctuations phase correlations

reactions

single particle transfer, e.g.  $(p, d)$

$$\frac{2R}{d} \approx 10$$

absolute cross section reflects  
the full nucleon probability  
amplitude distribution, and does  
not depend of the specific choice  
of  $v_{np}$

Cooper pair transfer, e.g.  $(p, t)$

$$\frac{2R}{a} \approx 10$$

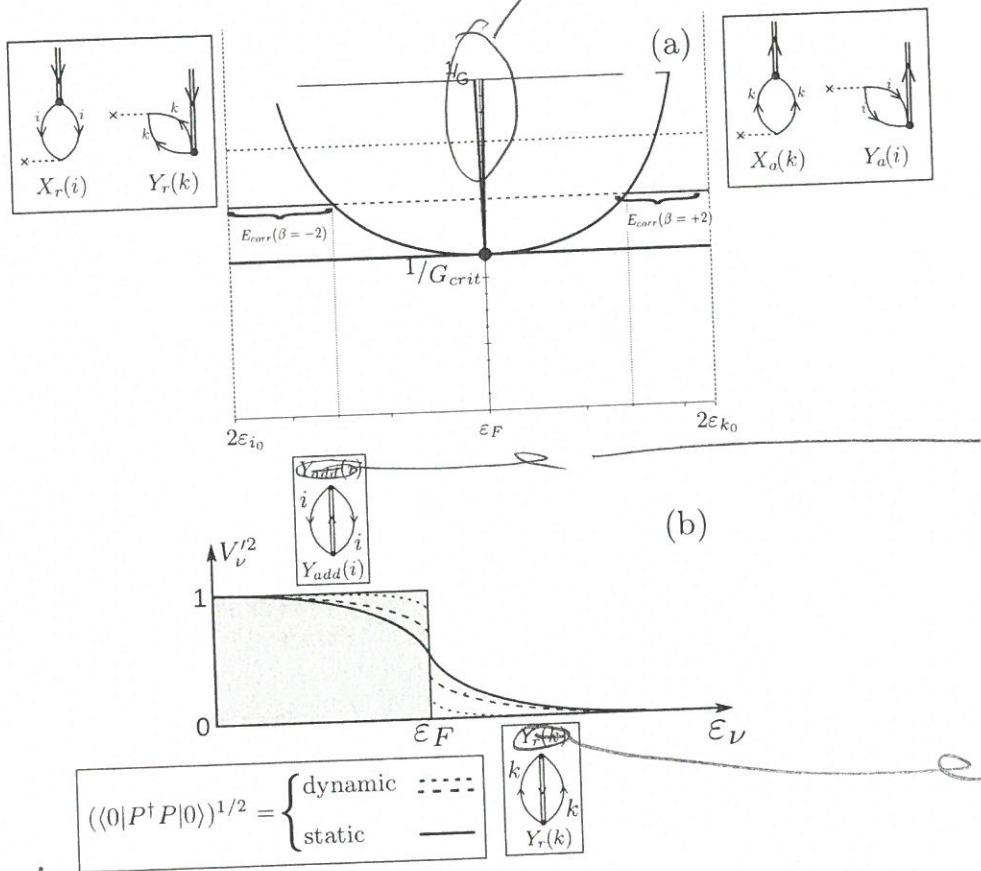
leaves space

Successive and simultaneous  
transfer amplitude contributions to  
the absolute cross section carry in a  
equal efficient manner information  
concerning pair correlations

Figure 2.4.2: Classical localization and zero point fluctuations, associated with independent-particle (normal density) and independent-pair motion (abnormal density).

## 2.5. PAIR VIBRATION SPECTROSCOPIC AMPLITUDES

please



✓ Figure 2.5.6: Schematic representation of the quantal phase transition taking place as a function of the pairing coupling constant in a (model) closed shell nucleus. (a) dispersion relation associated with the RPA diagonalization of the Hamiltonian  $H = H_{sp} + H_p$  for the pair addition and pair removal modes. In the insets are shown the two-particle transfer processes exciting these modes, which testify to the fact that the associated zero point fluctuations (ZPF) which diverge at  $G = G_{crit}$ , blur the distinction between occupied and empty states typical of closed shell nuclei. (b) occupation number associated with the single-particle levels. For  $G < G_{crit}$ , there is a dynamical depopulation (population) of levels  $i(k)$  below (above) the Fermi energy. For  $G > G_{crit}$ , the deformation of the Fermi surface becomes static, although with a non-vanishing dynamic component (cf. Fig. 2.1.2).

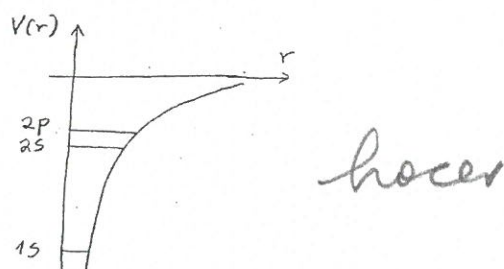


Figure 2.D.1: Schematic representation of the lowest single-particle levels in which the electron can move in a hydrogen atom.

Within the present context, an atom violates translational invariance as its center of mass (CM) occupies a definite position in space defining a privileged origin for a reference frame. Setting both ions and electrons in uniform motion through a Galilean transformation restores symmetry, the inertia being the total mass! Thus, when one pushes the system on one end it starts moving as a rigid body (generalized rigidity), without the need of propagation of information through it.

Such a motion (isoscalar in the case of the atomic nuclei, where  $N$  and  $Z$  move in phase, equivalent to electrons and ions doing so in the case of condensed or soft matter) display zero restoring force. Thus, the associated ZPF diverge requiring, quantum mechanically, a state orthogonal to it in which the two types of constituents particles (electrons and ions, neutrons and protons), move out of phase. Such a state is, in the nuclear case<sup>102</sup> the GDR and corresponds to a mode in which protons and neutrons slosh back and forth out of phase (isovector mode), a situation which is similar to that of atomic clusters (Mie resonance). In the atomic or molecular case these states (dipole vibration of electrons against the positive ions) are rather directly related to the single-electron atomic shell physics ( $1s \rightarrow 2p$  transition in the case of the H atom). Two atoms displaying the above ZPF will interact through van der Waals (dispersive, retarded) interaction.

### 2.D.1 van der Waals interaction between two hydrogen atoms

For large values of the internuclear distance  $r_{AB} = R$ , the exchange phenomenon is unimportant (Pauli principle) and one can take as the unperturbed wavefunction for a system of two hydrogen atoms (Fig. 2.D.1) the simple product of two hydrogenlike wavefunctions,

$$\Psi^0 = u_{1sA}(1)u_{1sB}(2). \quad (2.D.1)$$

The perturbation for this wavefunction arises from the potential energy terms

<sup>102</sup>Note however the pygmy halo resonance, soft  $E1$ -mode in the neutron halo nuclei like  $^{11}\text{Li}$ , which essentially forces a permanent dipole in the  $|^{11}\text{Li}_{(gs)}\rangle$ .

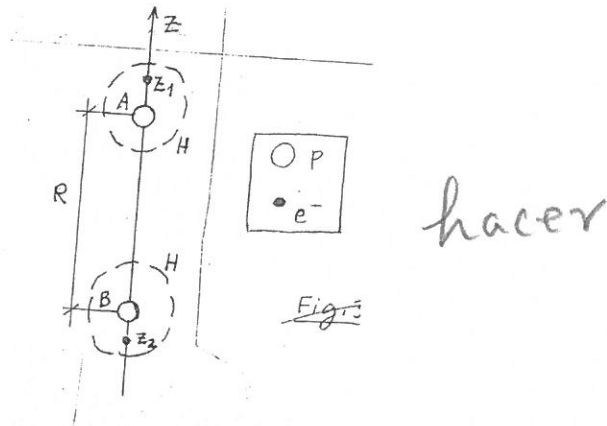


Figure 2.D.2: Planar configuration assumed for two hydrogen atoms at a relative distance  $R$ .

$$H' = \frac{e^2}{r_{12}} + \frac{e^2}{r_{AB}} - \frac{e^2}{r_{A2}} - \frac{e^2}{r_{B1}}, \quad (2.D.2)$$

corresponding to the variety of Coulomb interactions involving electrons and protons. Let us assume for simplicity that we are dealing with a one-dimensional problem, in which case one can write (Fig. 2.D.2)

$$\begin{aligned} \mathbf{r}_{12} &= (R + z_1 + z_2) \hat{z}, \\ \mathbf{r}_{AB} &= R \hat{z}, \\ \mathbf{r}_{A2} &= (R + z_2) \hat{z}, \\ \mathbf{r}_{B1} &= (R + z_1) \hat{z}. \end{aligned} \quad (2.D.3)$$

Because all these distances are much larger than the radius of the atom ( $a_0 \approx 0.529 \text{ \AA}$ , Bohr radius) the expression (2.D.2) can be calculated making use of a Taylor expansion, and diagonalize it with the help of perturbation theory. One obtains

$$r_{12}^2 = (R + z_1 + z_2)^2 = R^2 \left[ 1 + 2 \frac{(z_1 + z_2)}{R} + \frac{(z_1 + z_2)^2}{R^2} \right], \quad (2.D.4)$$

which leads to

$$\frac{e^2}{r_{12}} = \frac{e^2}{R \left[ 1 + \frac{2(z_1 + z_2)}{R} + \frac{(z_1 + z_2)^2}{R^2} \right]^{1/2}} \approx \frac{e^2}{R} \left[ 1 - \frac{(z_1 + z_2)}{R} - \frac{(z_1 + z_2)^2}{2R^2} \right]. \quad (2.D.5)$$

Similarly

$$r_{A2}^2 = (R^2 + 2Rz_2 + z_2^2) = R^2 \left( 1 + 2 \frac{z_2}{R} + \frac{z_2^2}{R^2} \right), \quad (2.D.6)$$

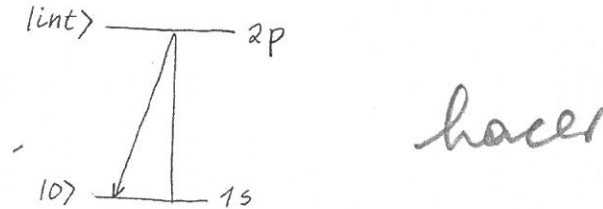


Figure 2.D.3: Schematic representation of the virtual processes associated with (2.D.14).

and thus

$$D_{en} = E_{int} - E_0 = \frac{e^2}{2a_0} = 1 \text{ Ry} = 13.606 \text{ eV}. \quad (2.D.16)$$

One can then write

$$\begin{aligned} \Delta E_z^{(2)} &= -\frac{|\langle 0|H'|0\rangle|^2}{D_{en}} = -\frac{e^4}{R^6} \frac{|\langle 0|z_1^2 z_2^2|0\rangle|^2}{D_{en}}, \\ &= -\frac{e^4}{R^6} \frac{\int d\tau_1 d\tau_2 u_{1s}^2(1) u_{1s}^2(2) z_1^2 z_2^2}{D_{en}}, \\ &= -\frac{e^4}{R^6} \frac{\int d\tau_1 \rho(z_1) z_1^2 \int d\tau_2 \rho(z_2) z_2^2}{D_{en}}, \\ \overline{z}_2^2 &\quad \overbrace{=} -\frac{e^4}{R^6} \frac{\overline{z}_1^2}{D_{en}} = -\frac{e^4}{R^6} \frac{a_0^2 a_0^2}{\frac{e^2}{2a_0}} = -\frac{2e^2 a_0^5}{R^6}. \end{aligned} \quad (2.D.17)$$

This result corresponds to the  $z$ -degree of freedom of the system (two H atoms at a distance  $R \gg a_0$ ). One has thus to multiply the above result by 3 to take into account the  $x$  and  $y$  degrees of freedom. Thus

$$\Delta E^{(2)} = -\frac{6e^2 a_0^5}{R^6}. \quad (2.D.18)$$

Let us now calculate the van der Waals interaction between two H-atoms at a distance of the order of ten times the summed radii of the two atoms ( $\approx 2a_0 \approx 1 \text{ \AA}$ ), that is for  $R \approx 10 \text{ \AA}$ ,

$$\begin{aligned} \Delta E_{H-H}^{(2)}(10 \text{ \AA}) &\approx -\frac{6 \times 14.4 \text{ eV \AA}(0.529 \text{ \AA})^5}{(10 \text{ \AA})^6} \\ &\approx -3.6 \times 10^{-6} \text{ eV} = -3.6 \mu\text{eV} \end{aligned} \quad (2.D.19)$$

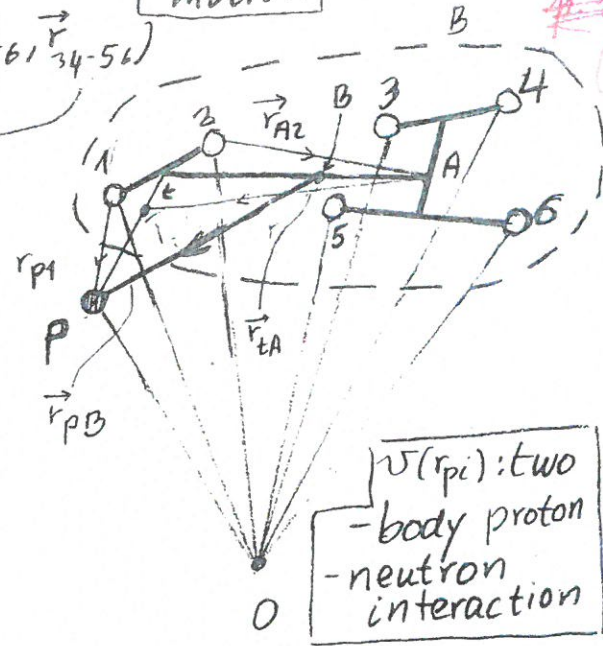
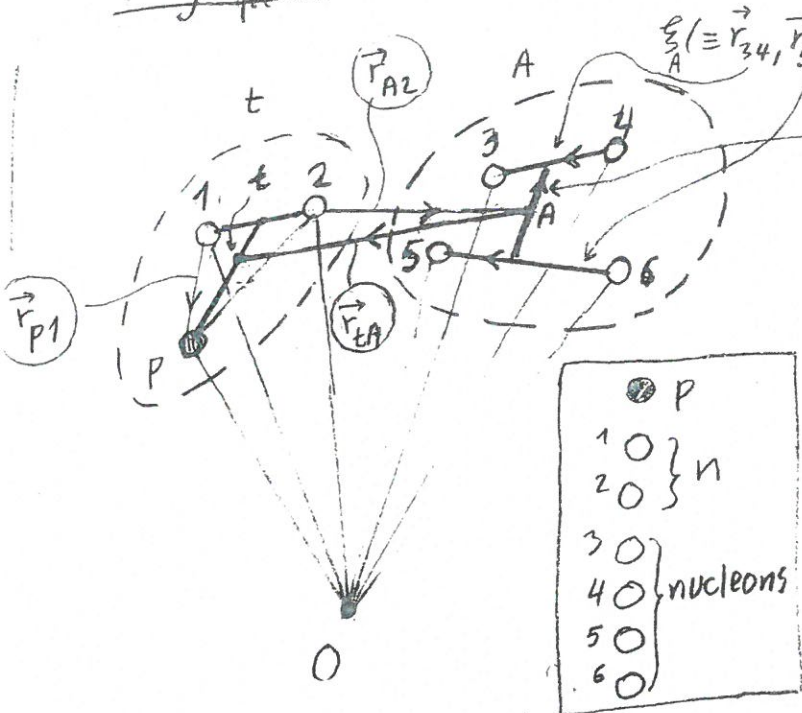
Making use of the relation

$$1 \text{ eV} = 2.42 \times 10^{14} \text{ Hz}, \quad (1 \text{ Hz} = \text{s}^{-1}) \quad (2.D.20)$$

Fig. 3.1.1

6 coordinates of relative motion

165  
(3) n



t + A  $\rightarrow$  P + B  
entrance channel exit channel

$$\Phi_t(\vec{r}_{p1}, \sigma_1, \vec{r}_{p2}, \sigma_2) \chi^{1/2}_{m_s}(\sigma_p) \psi_A(\xi_A) \chi^{(+)}_{tA}(\vec{r}_{tA}) \\ (\Phi_d(\vec{r}_{p1}, \sigma_1) \phi_d(\vec{r}_{p2}, \sigma_2) \chi^{1/2}_{m_s}(\sigma_p) \psi_A(\xi_A) \chi^{(+)}_{tA}(\vec{r}_{tA}))$$

$$\Psi_B(\xi_A, \vec{r}_{A1}, \sigma_1, \vec{r}_{A2}, \sigma_2) = \Psi_A(\xi_A) \sum_{\ell_1, j_1} [\Phi_{\ell_1, j_1}^{A+2}(\vec{r}_{A1}, \sigma_1, \vec{r}_{A2}, \sigma_2)]_0^0 \\ = \Psi_A(\xi_A) \sum_{nm} a_{nm} [\Phi_{n, \ell_1, j_1}^{A+2}(\vec{r}_{A1}, \sigma_1) \Phi_{m, \ell_2, j_2}^{A+2}(\vec{r}_{A2}, \sigma_2)]_0^0$$

First order  
in  $v$

$$(1) = 2 \sum_{\sigma_1, \sigma_2} \int d\xi_A d^3 r_{tA} d^3 r_{p1} \sqrt{\psi_A^*(\xi_A)} \sum_{\ell_1, j_1} [\Phi_{\ell_1, j_1}^{A+2}(\vec{r}_{A1}, \sigma_1, \vec{r}_{A2}, \sigma_2)]_0^0 \chi^{(-)*}(\vec{r}_{PB}) \chi^{1/2*}_{m_s}(\sigma_p) \mathcal{V}(\vec{r}_{p1}) \\ \times \Phi_t(\vec{r}_{p1}, \sigma_1, \vec{r}_{p2}, \sigma_2) \chi^{1/2}_{m_s}(\sigma_p) \psi_A(\xi_A) \chi^{(+)}_{tA}(\vec{r}_{tA})$$

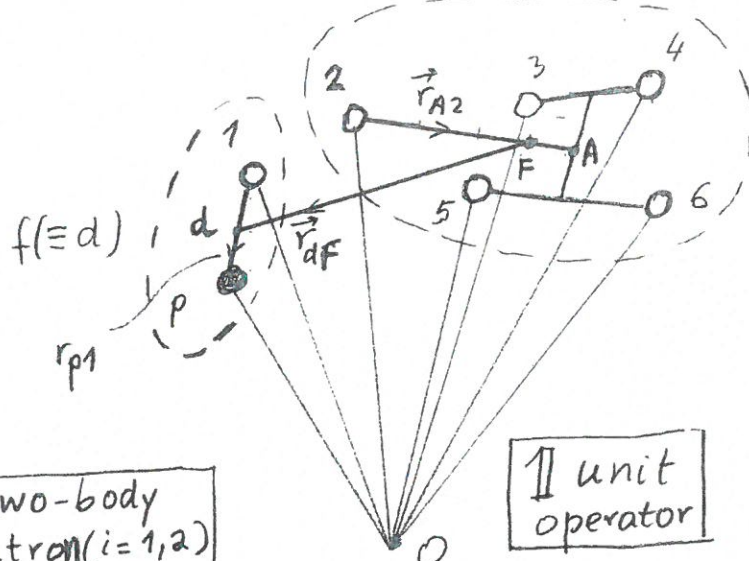
$$= 2 \sum_{\ell_1, j_1} \int d\xi_A d^3 r_{tA} d^3 r_{p1} d^3 r_{A2} [\Phi_{\ell_1, j_1}^{A+2}(\vec{r}_{A1}, \sigma_1, \vec{r}_{A2}, \sigma_2)]_0^0 \chi^{(-)*}_{PB}(\vec{r}_{PB}) \mathcal{V}(\vec{r}_{p1}) \\ \Phi_t(\vec{r}_{p1}, \sigma_1, \vec{r}_{p2}, \sigma_2) \chi^{(+)}_{tA}(\vec{r}_{tA})$$

Notice that the above expression violates two-nucleon sum rule transfer (i.e., it transfers more than two neutrons) by exactly  $T_{No.}^{(1)}$ , operative also in the independent particle limit.

Fig. 3.1.2

~~Fig. 3.1.2~~

$F(\equiv A+1)$  (4a)



$\mathcal{V}(r_{pi})$ : two-body proton-neutron ( $i=1,2$ ) interaction

1 P
2 O } n
3 O
4 O
5 O
6 O } nucleons

$f(\equiv d) + F(\equiv A+1)$   
intermediate channel

no distorted wave  
 $as(f, F)$  is a virtual channel with no asymptotic waves.  
thus 5 relative coordinates

$$\chi_{m_s}^{1/2}(\vec{r}_p) \phi_d(\vec{r}_{p1}, \sigma_1) \psi(\xi_A) \varphi_{\ell_f j_f m_f}^{A+1}(\vec{r}_{A2}, \sigma_2)$$

$$T^{(2)}_{succ} = 2 \sum_{\substack{\ell_1 j_1, \ell_F j_F, m_f, m_s, m_s' \\ \sigma_1 \sigma_2 \sigma_1' \sigma_2'}} \int d^3 r_{dF} d^3 r_{p1} d^3 r_{A2} \chi_{pB}^{(-)*}(\vec{r}_{pB}) \chi_{m_s}^{1/2*}(\vec{r}_B) \mathcal{V}(r_{p1}) \phi_d(r_{p1}, \sigma_1) \varphi_{\ell_f j_f m_f}^{A+1}(\vec{r}_{A2}, \sigma_2) \chi_{m_s}^{1/2}(\vec{r}_{pA}) \psi(\xi_A)$$

$$\times \frac{2 \mu_{dF}}{\hbar^2} \int d^3 r_{p1}' d^3 r_{A2}' d^3 r_{dF}' G(\vec{r}_{dF}, \vec{r}_{dF}') \chi_{m_s'}^{1/2*}(\vec{r}_{p1}') \phi_d^{*}(\vec{r}_{p1}', \sigma_1') \psi(\xi_A') \varphi_{\ell_f j_f m_f}^{A+1}(\vec{r}_{A2}', \sigma_2') \mathcal{V}(r_{p2}')$$

$$\times \phi_t(\vec{r}_{p1}', \vec{r}_{p2}', \sigma_2') \chi_{m_s'}^{1/2}(\vec{r}_{p1}') \psi(\xi_A') \chi_{tA}^{(+)}(\vec{r}_{pA})$$

$$= 2 \sum_{\substack{\ell_1 j_1, \ell_F j_F, m_f \\ \sigma_1 \sigma_2 \sigma_1' \sigma_2'}} \int d^3 r_{dF} d^3 r_{p1} d^3 r_{A2} \chi_{pB}^{(-)*}(\vec{r}_{pB}) [\varphi_{\ell_1 j_1}^{A+2}(\vec{r}_{A1}, \sigma_1, \vec{r}_{A2}, \sigma_2)]_0^0 \mathcal{V}(r_{p1}) \phi_d(r_{p1}, \sigma_1) \varphi_{\ell_f j_f m_f}^{A+1}(\vec{r}_{A2}, \sigma_2)$$

$$\times \frac{2 \mu_{dF}}{\hbar^2} \int d^3 r_{p1}' d^3 r_{A2}' d^3 r_{dF}' G(\vec{r}_{dF}, \vec{r}_{dF}') \phi_d^{*}(\vec{r}_{p1}', \sigma_1') \varphi_{\ell_f j_f m_f}^{A+1}(\vec{r}_{A2}', \sigma_2') \mathcal{V}(r_{p2}') \phi_d(r_{p1}', \sigma_1') \phi_d(r_{p2}', \sigma_2') \chi_{tA}^{(+)}(\vec{r}_{pA})$$

First order in  $\mathcal{V}$

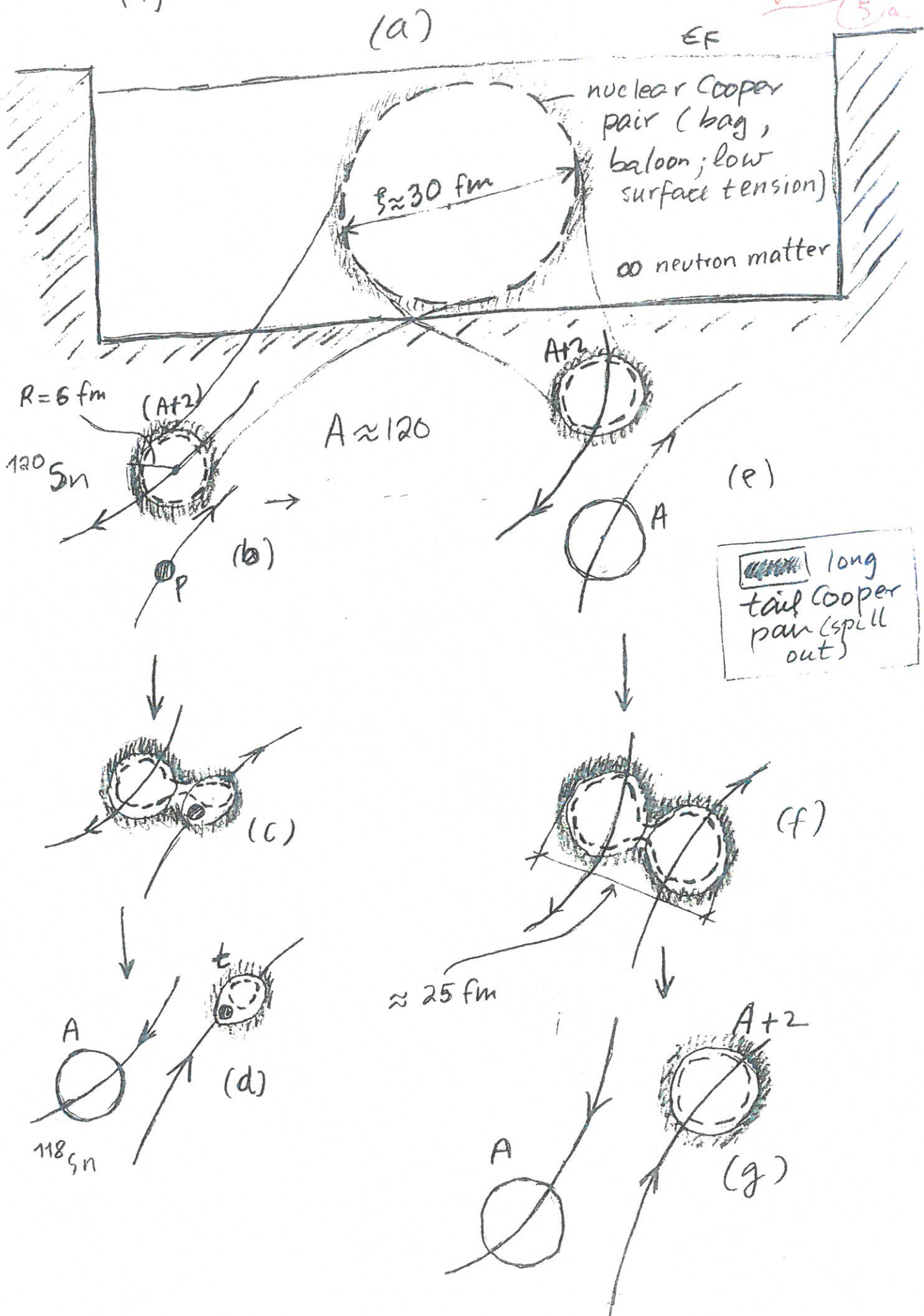
$$T^{(1)}_{NO} = 2 \sum_{\substack{\ell_1 j_1, \ell_F j_F \\ m_s m_s'}} \int d^3 r_{dF} d^3 r_{p1} d^3 r_{A2} \chi_{pB}^{(-)*}(\vec{r}_{pB}) \chi_{m_s}^{1/2*}(\vec{r}_B) \psi(\xi_B) \mathcal{V}(r_{p1}) \phi_d(r_{p1}, \sigma_1) \varphi_{\ell_f j_f m_f}^{A+1}(\vec{r}_{A2}, \sigma_2) \chi_{m_s}^{1/2}(\vec{r}_{pA}) \psi(\xi_A)$$

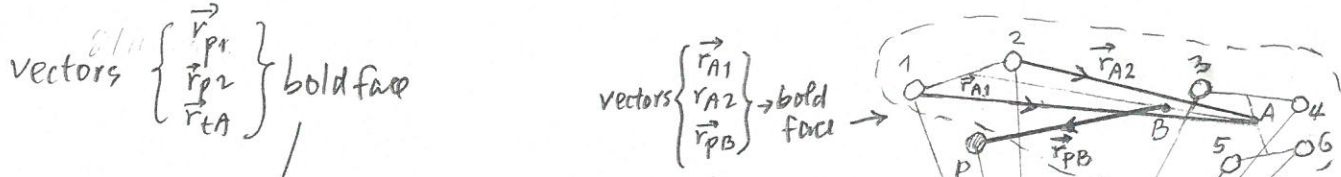
$$\times \underbrace{\int d^3 r_{p1} d^3 r_{A2} d^3 r_{dF} \chi_{m_s}^{1/2*}(\vec{r}_{p1}) \phi_d^{*}(\vec{r}_{p1}, \sigma_1') \psi(\xi_A') \varphi_{\ell_f j_f m_f}^{A+1}(\vec{r}_{A2}, \sigma_2')}_{6 \text{ relative coords.}}$$

$$= 2 \sum_{\substack{\ell_1 j_1, \ell_F j_F \\ m_s m_s'}} \int d^3 r_{dF} d^3 r_{p1} d^3 r_{A2} \chi_{pB}^{(-)*}(\vec{r}_{pB}) [\varphi_{\ell_1 j_1}^{A+2}(\vec{r}_{A1}, \sigma_1, \vec{r}_{A2}, \sigma_2)]_0^0 \mathcal{V}(r_{p1}) \phi_d(r_{p1}, \sigma_1) \varphi_{\ell_f j_f m_f}^{A+1}(\vec{r}_{A2}, \sigma_2)$$

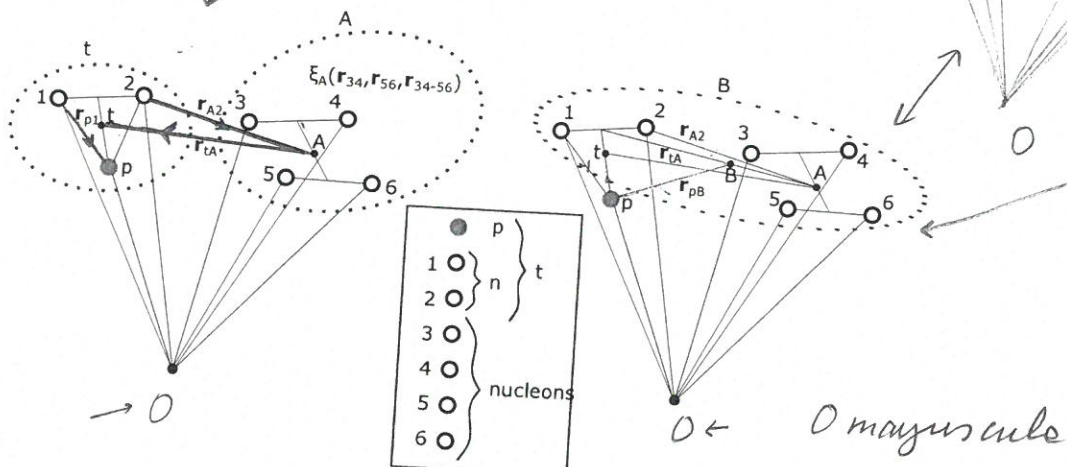
$$\times \int d^3 r_{p1}' d^3 r_{A2}' d^3 r_{dF}' \phi_d^{*}(\vec{r}_{p1}', \sigma_1') \varphi_{\ell_f j_f m_f}^{A+1}(\vec{r}_{A2}', \sigma_2') \mathbb{I} \phi_d(\vec{r}_{p1}', \sigma_1') \phi_d(\vec{r}_{p2}', \sigma_2') \chi_{tA}^{(+)}(\vec{r}_{pA})$$

Fig. 3.1.3





### 3.2. TRANSFER PROBABILITIES, ENHANCEMENT FACTOR



$$t + A \xrightarrow{\text{entrance channel}} p + B \xrightarrow{\text{exit channel}}$$

$$\frac{d\sigma}{d\Omega} = \frac{\mu_i \mu_f}{(2\pi\hbar^2)^2} \frac{k_f}{k_i} |T^{(1)} + T_{\text{succ}}^{(2)} - T_{NO}^{(1)}|^2$$

$$\phi_t(\mathbf{r}_{p1}, \sigma_1, \mathbf{r}_{p2}, \sigma_2) \chi_{m_i}^{1/2}(\sigma_p) \psi_A(\xi_A) \chi_{IA}^{(+)}(\mathbf{r}_{IA})$$

$$\chi_{m_i}^{1/2}(\sigma_p) \psi_B(\xi_B) \chi_{pB}^{(-)}(\mathbf{r}_{pB})$$

$$\Psi_B = \langle \Psi_{A+}(\xi_A, \mathbf{r}_{A1}, \sigma_1, \mathbf{r}_{A2}, \sigma_2) = \psi_A(\xi_A) \sum_{l_i j_i} [\phi_{l_i j_i}^{A+2}(\mathbf{r}_{A1}, \sigma_1, \mathbf{r}_{A2}, \sigma_2)]_0^0$$

$$= \psi_A(\xi_A) \sum_{nm} [a_{nm} \varphi_{n, l_i j_i}^{A+2}(\mathbf{r}_{A1}, \sigma_1) \varphi_{m, l_i j_i}^{A+2}(\mathbf{r}_{A2}, \sigma_2)]_0^0$$

$$T^{(1)} = 2 \sum_{\sigma_1, \sigma_2, \sigma_p} \int d\xi_A d\mathbf{r}_{IA} d\mathbf{r}_{p1} d\mathbf{r}_{A2} \psi_A(\xi_A) \sum_{l_i j_i} [\phi_{l_i j_i}^{A+2}(\mathbf{r}_{A1}, \sigma_1, \mathbf{r}_{A2}, \sigma_2)]_0^0$$

$$\times \chi_{pB}^{(-)}(\mathbf{r}_{pB}) \chi_{m_i}^{1/2}(\sigma_p) v(r_{p1}) \phi_t(\mathbf{r}_{p1}, \sigma_1, \mathbf{r}_{p2}, \sigma_2) \chi_{m_i}^{1/2}(\sigma_p) \psi_A(\xi_A) \chi_{IA}^{(+)}(\mathbf{r}_{IA})$$

$$= 2 \sum_{\sigma_1, \sigma_2, \sigma_p} \int d\mathbf{r}_{IA} d\mathbf{r}_{p1} d\mathbf{r}_{A2} \sum_{l_i j_i} [\phi_{l_i j_i}^{A+2}(\mathbf{r}_{A1}, \sigma_1, \mathbf{r}_{A2}, \sigma_2)]_0^0$$

$$\times \chi_{pB}^{(-)}(\mathbf{r}_{pB}) \chi_{m_i}^{1/2}(\sigma_p) v(r_{p1}) \phi_t(\mathbf{r}_{p1}, \sigma_1, \mathbf{r}_{p2}, \sigma_2) \chi_{m_i}^{1/2}(\sigma_p) \chi_{IA}^{(+)}(\mathbf{r}_{IA})$$

$\mathcal{V}(\vec{r}_{p1})$

✓ Figure 3.1.1: Contribution of simultaneous transfer, in first order DWBA, to the reaction  $A(t, p)B(\equiv A+2)$ . The nucleus  $A$  is schematically assumed to contain four nucleons, the triton being composed of two neutrons and one proton. The set of coordinates used to describe the entrance and exit channels are shown in the upper part, while in the lower part the simultaneous two-nucleon transfer amplitude is written in detail (cf. Potel, G. et al. (2013b)). It is of notice that the expression of  $T^{(1)}$  violates, in the independent particle basis used, the two-nucleon transfer sum rule by  $T_{NO}^{(1)}$ , amplitude operative also in lowest order of  $v$  (Fig. 3.1.2; see also App. 5.C.). It is of notice that of all the relative motion coordinates, only those describing the relative motion of  $(t, A)$  and of  $(p, B)$  have asymptotic values.

? check  
eventually  
eliminate )

(bold face vectors are the coordinate used to describe the relative motion, while the intrinsic coordinates  $\xi_A$  are the  $\vec{r}_{34}$ ,  $\vec{r}_{56}$  and  $\vec{r}_{34-56}$ )

The diagram illustrates a two-nucleon transfer process. At the top, a nucleus  $F(\equiv A+1)$  and a deuteron  $d(\equiv d)$  are shown. They interact via an intermediate channel  $f(\equiv d) + F(\equiv A+1)$ . The final state consists of a deuteron  $dF$  and a nucleus  $F(\equiv A+1)$ . Below the diagram, a legend identifies symbols:  $\bullet$  for  $p$ ,  $1 \circ$  for  $n$ ,  $2 \circ$  for  $n$ ,  $3 \circ$  for  $n$ ,  $4 \circ$  for nucleons, and  $5 \circ$  and  $6 \circ$  for nucleons.

Below the diagram, the amplitude  $T_{\text{succ}}^{(2)}$  is given by:

$$T_{\text{succ}}^{(2)} = 2 \sum_{l_i, l_f, j_f, m_f} \sum_{\sigma_1 \sigma_2} \int d\xi_A dr_{df} dr_{p1} dr_{A2} \chi_{pB}^{(-)*}(\xi_B) \psi_d(r_{p1}) \phi_d(r_{p1}) \varphi_{l_f, j_f, m_f}^{A+1}(r_{A2}, \sigma_2)$$

$$\times \chi_{m_s}^{1/2}(\sigma_p) \Psi_A(\xi_A) \frac{2\mu_{df}}{\hbar^2} \int d\xi'_A dr'_{df} dr'_{p1} dr'_{A2} G(r_{df}, r'_{df})$$

$$\times \chi_{IA}^{(+)}(r_{IA}) \psi_A^{(-)*}(\xi_A) \psi_d(r'_{p1}) \phi_d(r'_{p1}) \varphi_{l_f, j_f, m_f}^{A+1}(r'_{A2}, \sigma'_2)$$

$$= 2 \sum_{l_i, l_f, j_f, m_f} \sum_{\sigma_1 \sigma_2} \int dr_{df} dr_{p1} dr_{A2} \chi_{pB}^{(-)*}(\xi_B) \psi_d(r_{p1}) \phi_d(r_{p1}) \varphi_{l_f, j_f, m_f}^{A+1}(r_{A1}, \sigma_1, r_{A2}, \sigma_2) \Big|_0^{(1)}$$

$$\times \frac{2\mu_{df}}{\hbar^2} \int dr'_{df} dr'_{p1} dr'_{A2} G(r_{df}, r'_{df}) \chi_{IA}^{(+)}(r'_{IA}) \psi_d(r'_{p1}) \phi_d(r'_{p1}, \sigma'_1) \phi_d(r'_{p2}, \sigma'_2) \varphi_{l_f, j_f, m_f}^{A+1}(r'_{A2}, \sigma'_2)$$

*insert corrected formulae p. 376*

*NO apparent error (180) Ex C82 PRC 82*

*Y 54321-9*

*2μ df / h²*

*T<sub>NO</sub><sup>(1)</sup>*

*T<sub>NO</sub><sup>(2)</sup>*

*T<sub>NO</sub><sup>(2)</sup>*

Figure 3.1.2: Successive and non-orthogonality contributions to the amplitude describing two-nucleon transfer in second order DWBA, entering in the expression of the absolute differential cross section  $d\sigma/d\Omega = \frac{\mu_i \mu_f}{(4\pi\hbar^2)^2} \frac{k_f}{k_i} |T^{(1)} + T_{\text{succ}}^{(2)} - T_{\text{NO}}^{(2)}|^2$ . Concerning  $T^{(1)}$  we refer to Fig. 3.1.1. In the upper part of the figure the coordinates used to describe the intermediate channel  $d + F(\equiv A + 1)$  are given, while in the lower part the responding expressions are displayed (Potel, G. et al., 2013b) in the case of a  $(t, p)$  process. Schematically, the three contributions  $T^{(1)}$ ,  $T_{\text{succ}}^{(2)}$  and  $T_{\text{NO}}^{(2)}$  to the transfer amplitude can be written as  $\langle pB|v|tA \rangle$ ,  $\sum \langle pB|v|dF \rangle \langle dF|v|tA \rangle$  and  $\sum \langle pB|v|dF \rangle \langle dF|1|tA \rangle$  respectively, where  $v$  is the proton-neutron interaction and  $1$  the unit operator. Within this context, while  $T_{\text{NO}}^{(2)}$  receives contributions from the intermediate (virtual) closed  $(d + F)$  channel as  $T_{\text{succ}}^{(2)}$  does, it is first order in  $v$  as  $T^{(1)}$ .

*(bold face vectors are the ~~described~~ used to describe the relative motion while the ~~intrinsic~~ coordinates  $\vec{r}_{34}$  are  $\vec{r}_{34}, \vec{r}_{56}$  and  $\vec{r}_{34-56}$ )*

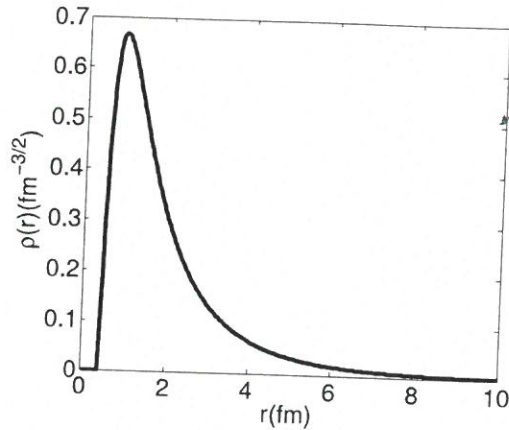


Figure 5.1.2: Radial wavefunction  $\rho_d(r)$  (hard core 0.45 fm) entering the deuteron wavefunction (cf. Tang and Herndon (1965)).

$$T_{succ}^{(2)}(\theta) = 2 \sum_{l_i, j_i} \sum_{l_f, j_f, m_f} \sum_{\sigma_1 \sigma_2} \int d\mathbf{r}_{dF} d\mathbf{r}_{p1} d\mathbf{r}_{A2} [\phi_{l_i, j_i}^{A+2}(\mathbf{r}_{A1}, \sigma_1, \mathbf{r}_{A2}, \sigma_2)]_0^{0*} \chi_{pB}^{(-)*}(\mathbf{r}_{pB}) v(\mathbf{r}_{p1}) \\ \times \phi_d(\mathbf{r}_{p1}) \varphi_{l_f, j_f, m_f}^{A+1}(\mathbf{r}_{A2}) \int d\mathbf{r}'_{dF} d\mathbf{r}'_{p1} d\mathbf{r}'_{A2} G(\mathbf{r}_{dF}, \mathbf{r}'_{dF}) \\ \times \phi_d(\mathbf{r}'_{p1})^* \varphi_{l_f, j_f, m_f}^{A+1*}(\mathbf{r}'_{A2}) \frac{2\mu_{dF}}{\hbar^2} v(\mathbf{r}'_{p2}) \phi_d(\mathbf{r}'_{p1}) \phi_d(\mathbf{r}'_{p2}) \chi_{IA}^{(+)}(\mathbf{r}'_{IA}), \quad (5.1.5b)$$

$$T_{NO}^{(2)}(\theta) = 2 \sum_{l_i, j_i} \sum_{l_f, j_f, m_f} \sum_{\sigma_1 \sigma_2} \int d\mathbf{r}_{dF} d\mathbf{r}_{p1} d\mathbf{r}_{A2} [\phi_{l_i, j_i}^{A+2}(\mathbf{r}_{A1}, \sigma_1, \mathbf{r}_{A2}, \sigma_2)]_0^{0*} \chi_{pB}^{(-)*}(\mathbf{r}_{pB}) v(\mathbf{r}_{p1}) \\ \times \phi_d(\mathbf{r}_{p1}) \varphi_{l_f, j_f, m_f}^{A+1}(\mathbf{r}_{A2}) \int d\mathbf{r}'_{p1} d\mathbf{r}'_{A2} d\mathbf{r}'_{dF} \phi_d(\mathbf{r}'_{p1}) \phi_d(\mathbf{r}'_{p2}) \chi_{IA}^{(+)}(\mathbf{r}'_{IA}), \quad (5.1.5c)$$

The quantities  $\mu_i, \mu_f (k_i, k_f)$  are the reduced masses (relative linear momenta) in both entrance (initial,  $i$ ) and exit (final,  $f$ ) channels, respectively. In the above expressions,  $\varphi_{l_f, j_f, m_f}^{A+1}(\mathbf{r}_{A1})$  are the wavefunctions describing the intermediate states of the nucleus  $F (\equiv (A + 1))$ , generated as solutions of a Woods-Saxon potential,  $\phi_d(\mathbf{r}_{p2})$  being the deuteron bound wavefunction (see Fig. 5.1.2). Note that some or all of the single-particle states described by the wavefunctions  $\varphi_{l_f, j_f, m_f}^{A+1}(\mathbf{r}_{A1})$  may lie in the continuum (case in which the nucleus  $F$  is loosely bound or unbound). Although there are a number of ways to exactly treat such states, discretization processes may be sufficiently accurate. They can be implemented by, for example, embedding the Woods-Saxon potential in a spherical box of sufficiently large radius. In actual calculations involving the halo nucleus  $^{11}\text{Li}$ , and where  $|F\rangle = |^{10}\text{Li}\rangle$ , one achieved convergence making use of approximately 20 continuum states and

write  
this  
in  
Fig.  
3.1.2  
p. 216

e.g.